Int. J. Electrochem. Sci., 15 **(2020)** 1964 – 1981, doi: 10.20964/2020.03.65

International Journal of
ELECTROCHEMICAL
SCIENCE
www.electrochemsci.org

Electrochemical Studies of Expired Drug (Formoterol) as Oilfield Corrosion Inhibitor for Mild Steel in H_2SO_4 Media

Xiangrong Ma[*], *Rui Dang*[*],*Yuhong kang, Ying Gong, Jiao Luo, Yuanyuan Zhang, Jiawei Fu, Chunyan Li, Yajun Ma*

School of Chemistry and Chemical Engineering, YuLin University, YuLin, Shaanxi, 719000 China.
[*]E-mail: dangrui8381@163.com, maxiangrong615@sina.com

Received: 7 November 2019 / *Accepted:* 31 December 2019 / *Published:* 10 February 2020

The expired drug Formoterol (EDF) [N-(2-hydroxy-5-(1-hydroxy-2-((1-(4-methoxyphenyl)propan-2-yl)amino)ethyl)phenyl)formamide] was examined as potential corrosion inhibitor of mild steel in 1 M sulphuric acid (H_2SO_4) media using weight loss, electrochemical and surface studies. Formoterol has its medicinal importance in traditional medicine as β2 receptor. It is known for its long lasting duration and can be effective till 12 hours. So, this expired drug is chosen as environment friendly corrosion inhibitor for mild steel in sulphuric acid, as it is easily available, cheap and easy to use. The weight loss results discovered that samples covered with Formoterol showed less weight loss compared to the samples without Formoterol. The electrochemical tests including electrochemical impedance spectroscopy (EIS), and potentiodynamic polarization (PDP) demonstrated good mitigation efficiency of Formoterol in 1 M H_2SO_4 media. The mixed shift of the anodic and cathodic slopes advised that the Formoterol represented as mixed category. The surface studies were completed using scanning electron microscopy (SEM) and contact angle. Both the studies displayed even surface in existence of Formoterol and rough surface in its absence. The kinetic and thermodynamic results including activation energy, enthalpy, and entropy were also obtained. Quantum simulations were done using Gaussian 9.0 software using density functional theory (DFT) to get computational parameters that can support the experimental findings. All the experimental results are in decent pact respectively.

Keywords: Formoterol, H_2SO_4, Mild steel, Inhibition, EIS, SEM

1. INTRODUCTION

Low carbon steel is used worldwide due to its cost, availability and large applications. Mild steel is an appropriate material for the tanks to store oil, pipelines to transport oil and gas, boilers, casing and tubing pipes for oil recovery [1]. To enhance oil recovery, the tanks are washed with acid solutions including hydrochloric and sulphuric acids. Sometimes, to remove the clogging or precipitations on the internal side of transportation pipelines they are treated with acidic solutions. These acidizing solutions

may cause severe corrosion in the storage tanks, pipelines or oilfield reservoir [2]. This could further lead to accidents, failures and complete shutdown of the place. Internal corrosion is very difficult to measure or to keep a regular watch as the blisters can develop beneath the coating of the pipeline and can grow severely with time. The depth of the pitting or uniform corrosion will increase extensively if not treated well in time. The corrosion will start to form more pits and cracks throughout the area leading to the failures and accidents. So, there is always a need to develop compounds that can be mixed with acidizing solution to mitigate corrosion during the acidization process.

Although, many corrosion mitigating technique exists, but use of inhibitors is widely used and best practice to effectively mitigate corrosion process. It is of both pragmatic and theoretical importance. Inhibitors are used in pickling, descaling and cleaning processes to diminish the corrosion rate of the metals. Now, due to strict regulation from the governments and environment regulatory boards the existing compounds cannot be used in higher concentration due to their toxicity level. Adding these substances in lower concentration may not work always depending on the size of the tanks. It is cheap, easily applicable and requires simple instruments. So in order to develop and test ecofriendly compounds, extraction of substances from plants being natural, without toxicity was conducted. Several authors have conduced similar tests and have obtained good results as oilfield inhibitor [3-10]. The achieved results exhibited that plant extracts could function as potential corrosion inhibitors.

Previous works have indicated the good potential of organic compounds as inhibitors to mitigate corrosion [11-16]. The organic compounds contain π bonds, benzene rings, conjugated double bonds, and heteroatoms (N, S, O, P) that makes them very efficient. A wide class of drugs have similar structures to these carbon-based complexes including pyridines, furans, imidazoles, thiophenes, isoxazoles etc. [17-20]. This distinguished feature is the motivation worldwide to study the potential of drugs as corrosion inhibitors. Being eco-friendly, and non-toxic, drugs ideally suit the environmental regulations over the toxic inhibitors. Therefore, a number of research work is done using new and expired medications as corrosion inhibitors [21-25]. The outcome of using the expired drugs were surprising as they prove to be ideal and cost effective corrosion inhibitors than being a pharmaceutical compound that needs to be disposed of [26-28].

Formoterol (EDF), also recognized as eformoterol, is a long-acting β2 agonist (LABA) used as a bronchodilator in the controlling of asthma. It has an prolonged length of action (up to 12 h) related to short-acting β2 agonists such as salbutamol (albuterol), those are only suitable for 4 h to 6 h. Agonists such as Formoterol are recommended as "symptom controllers" to increase prophylactic corticosteroid treatment. However, a short duration agonist also referred as “reliever” like salbutamol is still needed, since LABAs are not recommended for the treatment of acute asthma. The mechanism of action for Formoterol is by relaxing the smooth muscle in the airway so as to treat the exacerbation of asthma.

Structure and IUPAC name of EDF shown in Fig. 1. The present work explores the impeding outcome of Formoterol (EDF) on the mild steel corrosion in 1 M H_2SO_4 media using the weight loss, electrochemical and surface methods.

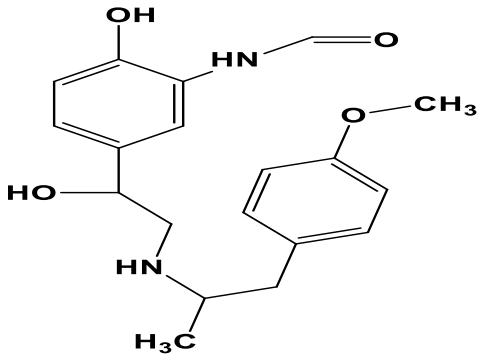

N-(2-hydroxy-5-(1-hydroxy-2-((1-(4-methoxyphenyl)propan-2-yl)amino)ethyl)phenyl)formamide

Figure 1. Structure and IUPAC name of Formoterol (EDF).

2. EXPERIMENTAL SECTION

The expired Formoterol (EDF) tablets were purchased from the pharmacy. It was weighed and powdered to fine particles. The powder was further solubilize in hot water and then refluxed with 1 M H_2SO_4 for 6 hours at 50 °C. The solid remnants on the filter paper were weighed and discarded. The solvent was further used for corrosion inhibition experiments.

Mild steel samples of specified dimensions were used for all the tests. The mild steel samples were prepared as test electrodes enclosed in epoxy resin with open 1 cm^2 area for electrochemical tests. The samples were abraded according to ASTM A262, and cleaned following the ASTM G-1 standard. The acidic solution of 1 M H_2SO_4 was organized from analytical rated H_2SO_4 and distilled water.

Gamry workstation was connected to the three cell installation with mild steel (working electrode), platinum electrode (auxiliary electrode) and saturated calomel electrode (reference electrode) to conduct the electrochemical tests. All the received data was analyses through Echem analyst software delivered by Gamry devices. EIS measurements were conducted under static conditions from 100 kHz to 0.01 Hz, with an amplitude of 10 mV. All potentials reported were measured in the range +250 mV – 250 mV versus reference electrode. Polarization tests were carried out at a scan rate of 1.0 mVs^{-1}. The tests were conducted when the system showed a stable potential with and without inhibitor. The efficiency of inhibition is obtained using the equation below:

$$\eta\% = \frac{R_{ct(inh)} - R_{ct}}{R_{ct(inh)}} \times 100 \quad (1)$$

Where $R_{ct(inh)}$ and R_{ct} be the charge transfer resistance with and without inhibitor in 1 M H_2SO_4 medium. The values of corrosion current density (I_{corr}) can be used to calculate the efficiency of inhibition (η %) through the equation below:

$$\eta\% = \frac{I_{corr} - I_{corr(i)}}{I_{corr}} \times 100 \quad (2)$$

Where I_{corr} and $I_{corr(i)}$ be the corrosion current density with and without inhibitor.

To test the hydrophillic and hydrophobic behavior of the steel surface, contact angle experiments were done using the drop technique. All the tests were performed using DSA100 Kruss instrument and

prior to each test the electrodes were cleaned cautiously to prevent contaminations. The scanning electron microscopy (SEM) was done to detect the changes at the external area of the metal. SEM was conducted using Tescan machine. The samples were washed with sodium bicarbonate solution to remove the corrosion products followed by distilled water prior to surface exposure.

Quantum simulations are done to support the experimental data with the theoretical parameters. Simulations were conducted using Gaussian 09 software and figures were obtained using Gauss view 5.0 software. Density function theory (DFT) method with B3LYP module was chosen for all atoms. Highest occupied molecular orbital (HOMO), Lowest unoccupied molecular orbital (LUMO), and dipole moment (μ) were investigated [29].

3. RESULTS AND DISCUSSION

3.1. Weight loss experiments

3.1.1 Effect of inhibitor concentration

The values of the inhibition efficiency (η%) achieved through weight loss experiments for diverse concentrations of EDF in 1 M H_2SO_4 are given in Table 1. The corrosion tests were executed on triplicate samples and their mean rate of corrosion was determined. The subsequent equation was followed to obtain the rate of corrosion (C_R) [30]:

$$C_R\,(\mathrm{mm/y}) = \frac{8.76W}{atD} \tag{3}$$

where W be the weight loss, a be the total area, t be the time of immersion (3 hours) and D be density of mild steel in (gcm^{-3}). The subsequent equation was used to determine the inhibition efficiencies (η%):

$$\eta\% = \frac{WL_b - WL_i}{WL_b} \times 100 \tag{4}$$

WL_i and WL_b are the corrosion rates with and without EDF, respectively.

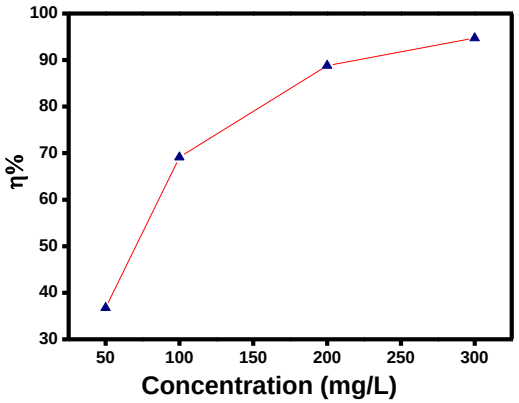

Figure 2. Effect of EDF concentration on inhibition efficiency .

The efficiency (η%) tend to rise with increase in the EDF concentration with rise in inhibitor concentration as exposed in Fig. 2 and Table 1. As inhibition efficiency can be correlated to the surface coverage, with escalation in efficiency surface coverage also increases. Maximum inhibition efficiency is found to be 95% for 300 mg/L EDF. The efficiency did not exceed much after the concentration was increased to 400 and 500 mg/L, so 300 mg/L is chosen as the optimum concentration for the EDF. The adsorption of EDF on the steel surface occurred through the heteroatoms present in the solution that formed a coating on the steel surface and blocked the acidic media [31].

Table 1. Corrosion data for mild steel in 1 M H_2SO_4 in the absence and presence of EDF.

Solution	Weight loss	C_R	η	Surf. Coverage
(mg/L)	(mg cm^{-2})	(mm y^{-1})	(%)	(θ)
1 M H_2SO_4	344	127.6	-	-
50	207	76.8	39	0.39
100	96	35.6	72	0.72
200	32	11.8	91	0.91
300	17	06.3	95	0.95

3.1.2. Effect of Immersion time

The effect of immersion time on the efficiency of EDF to inhibit mild steel corrosion in 1 M H_2SO_4 is revealed in Fig. 3. It is observed that the inhibition efficiency declines with growing time period from 2 to 8 hours. The phenomenon points that desorption of the EDF particles from metal surface occurs with rise in the time period. The corrosive solution of sulphuric acid is able to penetrate the inhibitor film and attack the steel surface.

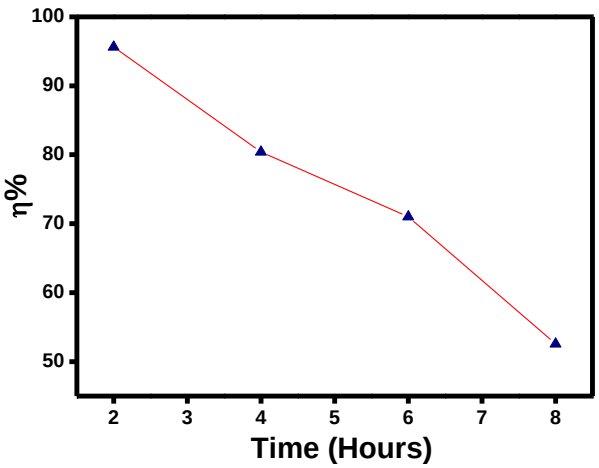

Figure 3. Effect of immersion time on corrosion of mild steel in 1 M H_2SO_4.

3.1.3. Effect of Acid concentration

The deviation in concentration of sulphuric acid was done from 0.5 to 2.0 M to analyze the change in the efficiency of EDF inhibitor as is exposed in Fig. 4. The inference is strong that with the modification in the concentration of acid from 0.5 M to 2.0 M, inhibition efficiency varied from 97.2% to 76.7%. The alteration in the efficiency with rising concentration of acid points toward the weak bonding of the EDF particles with steel surface or less effective nature that could be ruptured due to the presence of acidic media. It could also be deterred as with rise in acid concentration the concentration of the inhibitor used should also be increased for better inhibition efficiency.

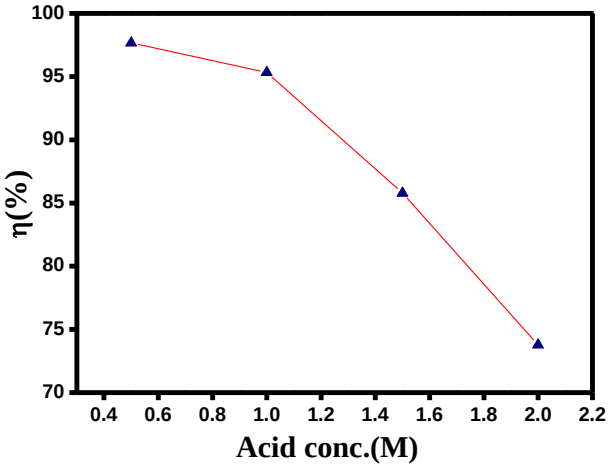

Figure 4. Influence of acid concentration from 0.5 to 2.0 M on corrosion of mild steel.

3.1.4. Effect of Temperature

The influence of temperature on the corrosion of mild steel in 1 M H_2SO_4 solution with and without 300 mg/L EDF was conducted using weight loss technique for a duration of 3 hours. The temperature was varied from 308 to 338 K.

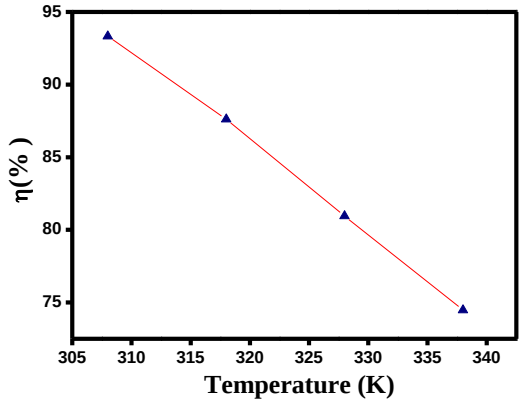

Figure 5. Effect of Temperature on corrosion of mild steel in 1 M H_2SO_4.

Fig. 5 shows the temperature versus inhibition efficiency and corrosion rate diagram. One can keenly observe from the figure that with a rise in temperatulm]kne the inhibition efficiency decreases and likewise the corrosion rate increases at optimum concentration (300 mg/L) of EDF. This decrease in inhibition efficiency at high temperature suggests that the EDF cannot perform at high temperature conditions. The increase in corrosion rate also points towards the aggressiveness of acidic solution at high temperatures. This may be due to desorption of the EDF particles from the mild steel surface that let the corrosive solution to attack the steel surface thereby increasing the rate of corrosion [32]. Also, it may be attributed to the thin film of the EDF that was removed or blistered at high temperature.

3.2 Adsorption isotherm

The Arrhenius equation given below was followed to obtain the activation energy of the electrochemical reaction [19]:

$$C_R = \lambda \exp\left(\frac{-E_a}{RT}\right) \quad (5)$$

where C_R represents the rate of corrosion, λ be the constant, E_a represents the activation energy, R be the gas constant, and T be the temperature. The values of log C_R (mpy) and 1/T x 10^{-3} (kelvin) were accounted for determination of activation energy as exposed in Fig. 6a. The transition state equation used is an alternative form of the Arrhenius equation [33]:

$$Rate = \frac{RT}{Nh}\exp\left(\frac{\Delta S^\circ}{R}\right)\exp\left(-\frac{\Delta H^\circ}{RT}\right) \quad (6)$$

where h represents Plank's constant, N be the Avogadro's number, $\Delta S°$ represents entropy and ΔH° represents enthalpy. A linear fit straight line is obtained from log (C_R/T) versus 1/T graph as exposed in Fig. 6b. The values of ΔS^o and ΔH^o were obtained from the slope and intercept as tabulated in table 2.

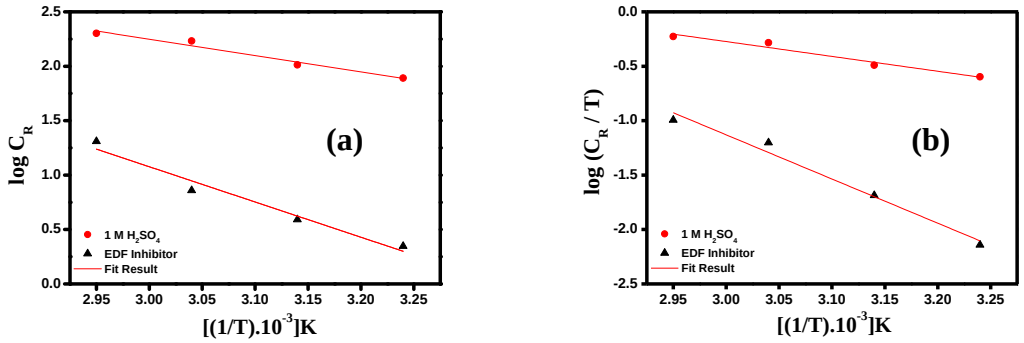

Figure 6. Arrhenius plots of (a) log C_R versus 1/T and (b) log C_R/T versus 1/T for mild steel in acidic media.

The data in Table 2 displays that activation energy (E_a) of mild steel in 1 M H_2SO_4 solution is greater in the presence of the EDF. On the other hand, it is lower in the acidic media without EDF inhibitor signifying that the inhibitor drops the inhibition efficiency at elevated temperature [34]. The value of activation energy (E_a), 23.3 kJ mol^{-1} for 1 M H_2SO_4 and 68.1 kJ mg^{-1} of 300 mg/L inhibitor was

obtained from the slope of the straight line. The greater value of E_a in presence of EDF is due to the very strong adsorption of EDF particles on the steel surface. The inhibitor formed a strong film/complex with the metal surface that reduced the dynamic centers and served as a protective layer [35]. The values obtained for free energy of adsorption (ΔG°_{ads}) shows a negative sign signifying the spontaneous nature of the corrosion process [36]. The equation below was used to determine the values [37].

$$\Delta G^{\circ}_{ads} = -RT\ln(55.5K) \quad (7)$$

Table 2. The thermodynamic parameters E_a, ΔH° and ΔS° for mild steel in 1 M H_2SO_4 with and without EDF.

EDF concentration (ppm)	E_a (kJ mol^{-1})	$-\Delta H^{\circ}$ (kJ mol^{-1})	$-\Delta S^{\circ}$ (J mol^{-1} K^{-1})	K_{ads} (M^{-1})	$-\Delta G^{\circ}_{ads}$ (kJ mol^{-1})
1 M H_2SO_4	23.3	18.1	132.4	07,988	-
50	31.2	22.3	102.1	14,083	31.4
100	52.2	39.4	83.4	16,187	32.1
200	63.4	52.1	57.5	19,551	34.3
300	68.1	65.4	31.4	23,986	35.2

$$K = \frac{\Theta}{C(1-\Theta)} \quad (8)$$

where, θ be the degree of coverage, C represents concentration of EDF in mol/L, R be the constant and T represents temperature. The ΔG°_{ads} value of the EDF is found to be -35.2 kJ/mol. This value is lesser than -40 kJ/mol demonstrating that EDF is adsorbed physically on the surface of mild steel [38]. The negative parameter of ΔG_{ads} specified the impulsive adsorption of EDF particles on the steel surface [39]. Higher values of K_{ads} represents better adsorption of the EDF particles on the steel surface as it is related to the free energy.

Chemical compounds establish corrosion mitigation by adsorption. The adsorption of EDF is inclined by the natural structures of molecules present in the solution, nature and external charge of metal, and type of acidic media [40]. The physical adsorption shows the electrically charged surface and charged particles in the acidic media. The steel surface consists of unoccupied d orbitals and lower energy orbital, through which it can form complex with the heteroatoms present in the EDF molecule [41].

The statistics for the physical phenomenon between the EDF particles and steel surface can be reflected by the isotherm of adsorption. The process is based on a chemical reaction where the EDF molecule displaces the water molecule present on the steel surface and get adsorbed [42].

$$Org_{(sol)} + xH_2O \rightarrow Org_{(ads)} + xH_2O_{(sol)} \quad (9)$$

where, $Org_{(sol)}$ and $Org_{(ads)}$ are the EDF particles in the solution and adsorbed particles on the steel surface, $H_2O_{(ads)}$ represents the water molecules, x be the size ratio. The surface coverage values determined through weight loss, impedance and polarization experiments were accounted to fit several isotherms of adsorption such as Flory Huggins, Langmuir, Temkin, and Frumkin. The good fit of these

isotherms can signify the nature of adsorption by the EDF molecules. Surface coverage (θ) can be correlated to the concentration of EDF inhibitor as shown below:

$$\theta = \frac{bC_{inh}}{1+bC_{inh}} \quad \text{(Langmuir isotherm)} \quad (10)$$

$$\exp(-2a\theta) = KC_{inh} \quad \text{(Temkin isotherm)} \quad (11)$$

where, b defines the adsorption, a represents molecular interaction, K be the equilibrium constant. Among all the isotherm of adsorption, Langmuir showed the best and linear fit to the surface coverage parameters as depicted in Fig. 7. The values of regression coefficient was close to 1 for all the experimental data that signifies the good adsorption of EDF particles on the steel in acidic media. All the acquired fits are in good agreement with each other.

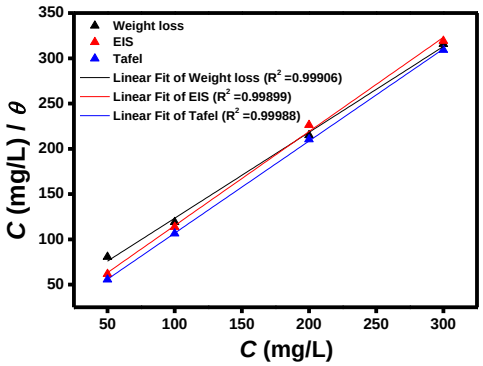

Figure 7. Linear fit results of Langmuir isotherm for adsorption of EDF on mild steel in 1 M H_2SO_4.

3.2 Electrochemical measurements

3.2.1. Electrochemical impedance spectroscopy (EIS) tests

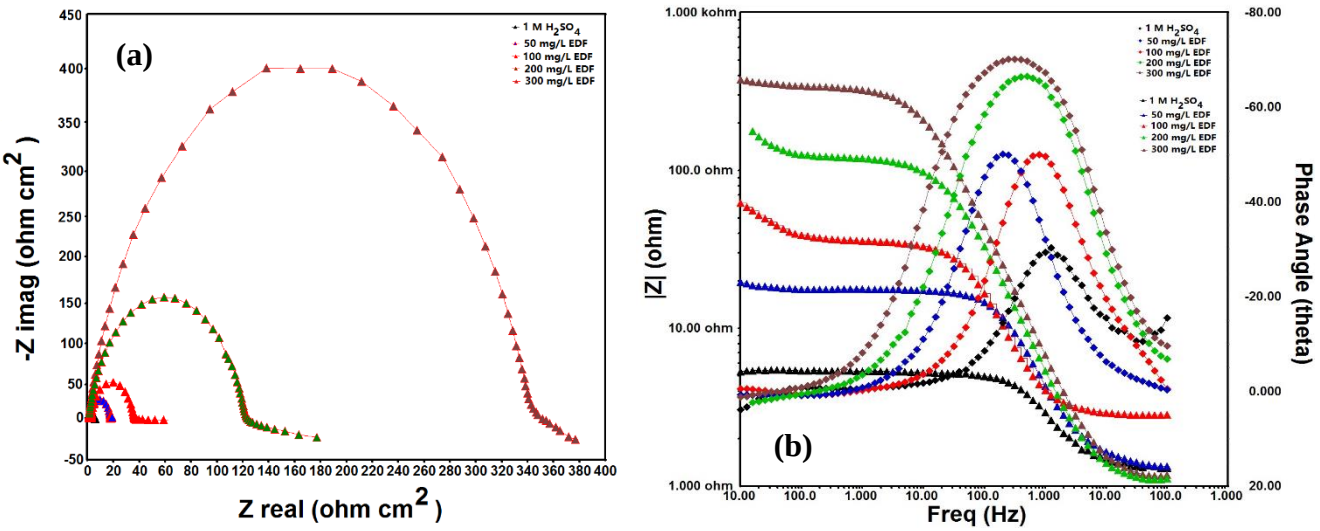

Figure 8. (a) Nyquist and (b) bode-phase angle plots for mild steel in 1 M H_2SO_4 with and without EDF at an amplitude of 10 mV.

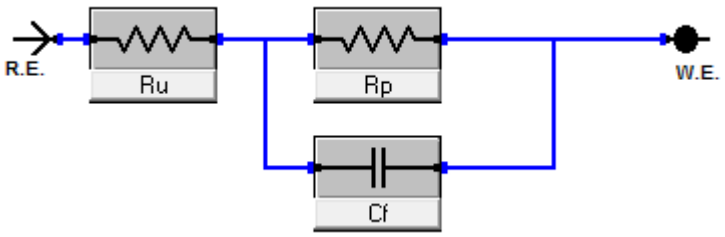

Figure 9. Corresponding Randle's circuit used to fit Nyquist plots in 1 M H_2SO_4 with various concentrations of EDF.

Nyquist figures of mild steel in 1 M H_2SO_4 with and without EDF are specified in Fig. 8a, and it can be detected that the width of the semicircle rises with increasing EDF adsorption. This rise in semicircles of capacitance recommends that the mitigation behavior of EDF is due to its good attachment with the mild steel surface deprived of varying the corrosion process [43-45]. Furthermore, Fig. 8a shows the higher and lower frequency regions with similar capacitance but with different diameter.

Table 3. Electrochemical impedance parameters for mild steel in 1 M H_2SO_4 solution with and without EDF at an amplitude of 10 mV.

Solutions(mg/L)	R_{ct} (Ω cm^2)	n	Yo ($10^{-6}\Omega^{-1}$ cm^{-2})	C_{dl} (μF cm^{-2})	η%	Slope	Phase angle (θ)
Blank	07.7	0.554	272.4	97.5	-	0.475	33.7
50	18.3	0.577	225.7	75.3	58	0.491	45.9
100	39.6	0.605	202.6	57.2	81	0.517	48.4
200	123.9	0.694	177.3	35.7	94	0.655	63.5
300	346.3	0.717	104.4	27.5	98	0.687	69.3

In the bode plots (Fig. 8b), the slope values tend to increase in existence of EDF than in its nonexistence (Table 3). This points toward the good inhibition action of EDF on mild steel surface. In phase angle plots (Fig. 8b), at the intermediate frequency the peak and phase angle values increases as the EDF concentration increases. The highest peak at 69.3° (300 mg/L) EDF concentration for mild steel was observed and reported in Table 3. This is an indication of the development of protective obstacle that blocks the acidic media [46]. In other words, presence of EDF film on the steel surface in acidic media increases its corrosion resistance property.

The obtained parameters of impedance after using the corresponding circuit (Fig. 9), are shown in Table 3. The Randle's equivalent circuit model contains capacitance CPE, which is in parallel with charge transfer resistance (R_{ct}) and overall in series with the solution resistance (R_s) [47]. The CPE impedance (Z_{CPE}) was obtained using the subsequent equation:

$$Z_{CPE} = Y_0[j\omega^{\alpha}]^{-1} \quad (12)$$

where j represents an imaginary number ($j = \sqrt{-1}$), Yo be the admittance for CPE, ω be the angular frequency, and α represents the phase change. The EDF leads to the variation of the capacitance parameters owing to the adsorption at the steel-liquid interface. The exact relation between the C_{dl} and CPE can be obtained by using the following equation [48]:

$$C_{dl} = Y_o^{1/\alpha}\left[\frac{1}{R_s} + \frac{1}{R_{ct}}\right]^{(\alpha-1)/\alpha} \quad (13)$$

According to the Table 3, the R_{ct} values rises and C_{dl} declines with the increase in EDF concentration to the acidic solution.The particular behavior can be attributed to the of EDF fragments all over the mild steel and reduces the straightforward connection between the metal and hostile media [49].

3.2.2. Polarization tests

Fig. 10 depicts the potentiodynamic polarization pictures of the mild steel with and without EDF in 1 M H_2SO_4 media. As can be seen from the figure that both the hydrogen evolution (cathodic) and steel dissolution (anodic) processes were affected after the accumulation of EDF in the acidic solution [50]. Although, the overall mechanism was not affected by the addition of the EDF as neither the anodic nor the cathodic shift was observed.

The little shift towards cathodic region after the addition of EDF, may be owing to the concept that the adsorption of EDF on the steel hindered the corrosive media attack on the working electrode as is evident from the $-\beta_c$ values reported in Table 4 [51]. So, the addition of EDF in the acidic media did not changed the overall mechanism of corrosion. There was also a little change in the anodic values of β_a that may be endorsed to the development of preventive layer of EDF molecules on the mild steel that further obstructed the progressive centers present on the steel, thereby slowing the dissolution process [52].

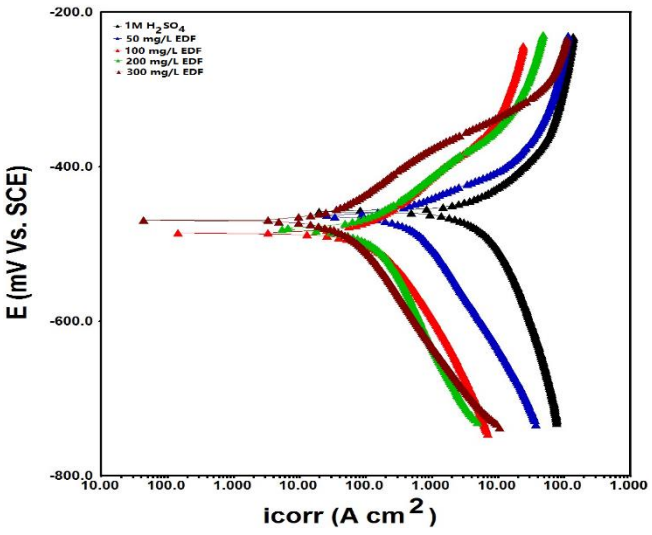

Figure 10. Polarization graph for mild steel in 1 M H_2SO_4 in presence and absence of EDF at a scan rate of 1 mV/S.

Table 4. Electrochemical polarization parameters for mild steel in 1 M H_2SO_4 solution with and without EDF at a scan rate of 1 mV/S.

EDF	E_{corr}	I_{corr}	β_a	β_c	η_p
(ppm)	(mV/SCE)	(mA cm^{-2})	(mV dec^{-1})	(mV dec^{-1})	(%)
1 M H_2SO_4	–427	277	89	155	–
50	–486	133	104	117	52
100	–496	72	72	94	74
200	–433	27	52	86	90
300	–421	15	44	97	95

The maximum inhibition efficiency of 95% at 300 mg/L concentration was observed suggesting the lower corrosion rate in presence of EDF. The corrosion potential did not showed much variation or shift and was quite stable. The conclusions of research papers suggests that if the shift or movement in corrosion potential is ≥ 85 mV with reference to the blank (1M H_2SO_4) solution, then only an EDF can be classified into anodic or cathodic inhibitor [53]. But, from Fig. 10 and Table 4, the shift is very evident and is found to be 75 mV. So, based on this theory EDF can be classified as mixed type EDF.

3.3 Surface Characterization

3.3.1. Contact Angle

To detect the surface behavior of mild steel with and without EDF, contact angle tests were conducted. Contact angle tests can provide essential information regarding the hydrophillic and hydrophobic nature of the steel. The samples were degreased and cleaned several times before test to remove all kinds of contaminants. A baseline establishment was completed after several attempts to perform the tests smoothly using the sessile drop technique. The solution was dropped using a syringe and was repeated for three times to make sure the reproducability of the tests. The 1 M H_2SO_4 solution without EDF recorded a lower contact angle of 11.6° as shown in Fig. 11. This may be endorsed to the surface of the steel that is in direct connection with the corrosive environment. The corrosive solution can directly attack the steel surface and due to this water loving nature it is termed as hydrophillic surface. Whereas, when the EDF was added in the solution, it formed a film at the steel surface and due to the presence of this film the contact angle begin to increase. It was 102.4° at 300 mg/L concentration suggesting that the film blocked the corrosive solution to reach at the steel surface and this nature is termed as hydrophobic behavior of the surface. So, the surface was hydrophillic without EDF and hydrophobic with EDF. This justifies the good inhibiting action of EDF in 1 M H_2SO_4.

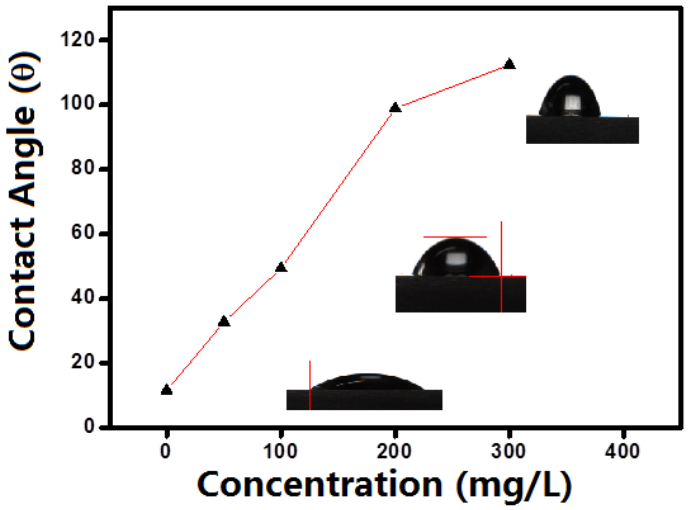

Figure 11. Contact angle for mild steel 1 M H_2SO_4 in presence and absence of EDF using sessile drop technology.

3.3.2 SEM characterization

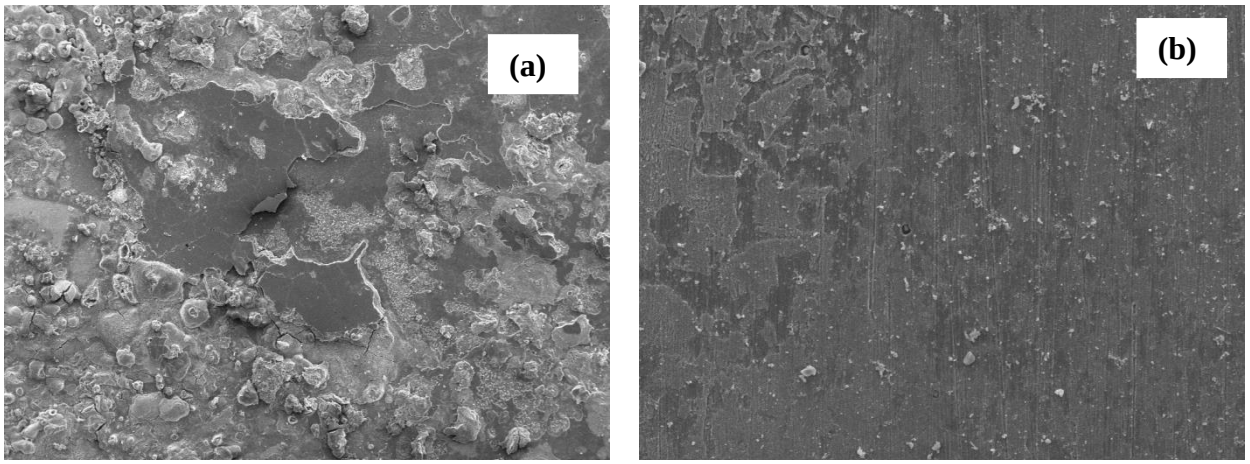

Figure 12. SEM images for mild steel in (a) 1 M H_2SO_4, and (b) in 300 mg/L EDF.

To observe the range of protection of the steel surface by EDF, the morphology of mild steel surface submerged in 1 M H_2SO_4 without and with 300 mg/L EDF was checked using SEM. In order to get a clear picture of EDF action the steel surface without EDF, SEM was conducted first and the result is represented in Fig. 12a. The surface is very rough, corroded and irregular. The corrosive solution attacked the mild steel surface and due to oxidation the steel formed rust after corroding. While, in presence of EDF the steel surface was smooth, regular and less corroded as shown in Fig. 12b. The abraded lines can be seen and the surface is much better than without EDF. This proposes that the EDF formed a shielding layer on the steel surface that inhibited the corrosion progression by blocking the corrosive solution from attacking the metal surface.

3.4. Quantum Chemical Investigations

The simulations were run to find the optimized geometry for the inhibitor. After the optimized geometry was obtained further studies were performed to get the detailed information about the molecular orbitals. The obtained computational structures are displayed in Fig. 13. Fig. 13a, 13b shows the optimized geometry of neutral and protonated EDF molecule, Fig. 13c, 13d show the highest occupied molecular orbital (HOMO) of neutral and protonated EDF molecule, Fig. 13e, 13f shows the lowest unoccupied molecular orbital (LUMO) structures of neutral and protonated EDF molecule, and Fig.13g, 13h shows the electronic charge distribution of neutral and protonated EDF molecule. Likewise, the obtained parameters including E_{HOMO}, E_{LUMO}, ΔE ($_{LUMO-HOMO}$), dipole moments (μ) are enumerated in Table 5. HOMO and LUMO represents the active sites through which the nucleophilic and electrophilic substitution reactions takes place. In other words, these sites provide the information about the electron donor and electron acceptor atoms in the inhibitor molecule.

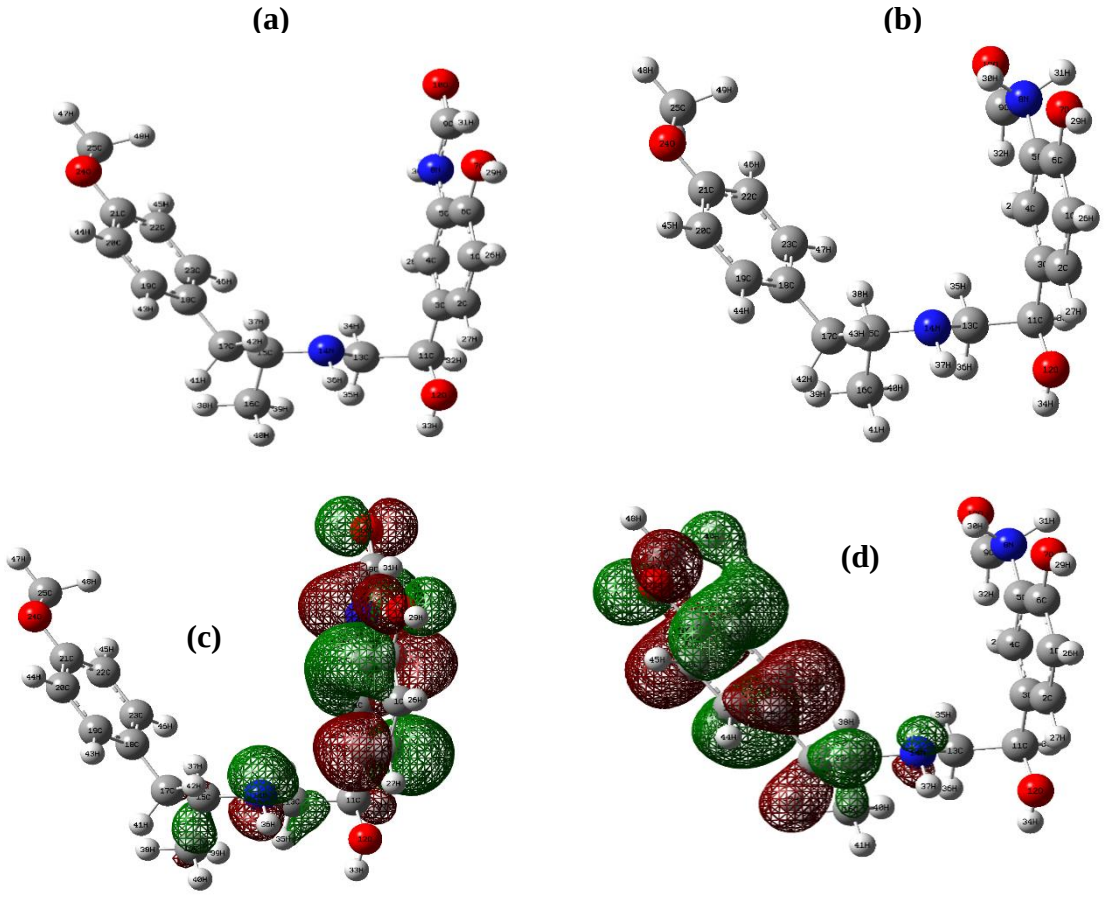

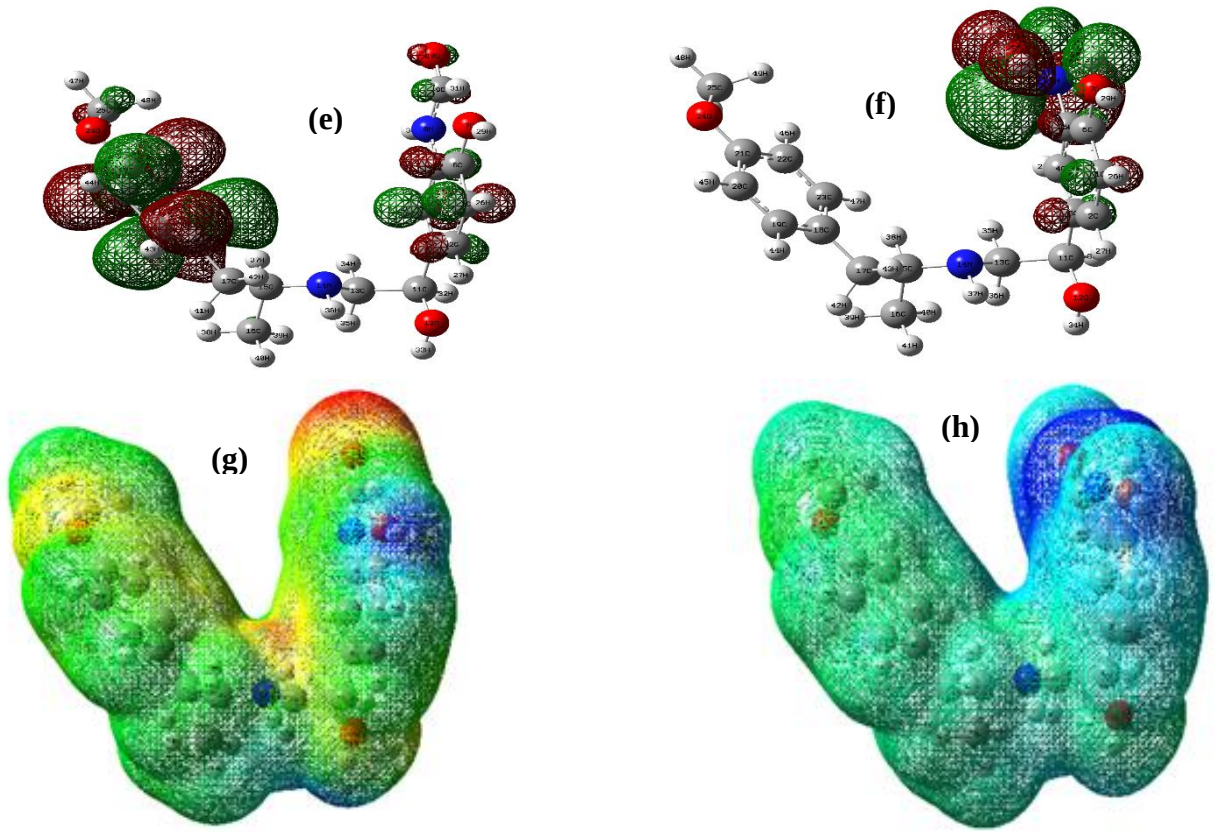

Figure 13. (a) Optimized molecular structure of neutral EDF (b) Optimized molecular structure of protonated EDF, (c) HOMO of neutral EDF (d) HOMO of protonated EDF (e) LUMO of neutral EDF (f) LUMO of protonated EDF (g) total charge density of neutral EDF and (h) total charge density of protonated EDF.

Table 5. All calculated computational parameters of EDF Inhibitor using Gaussian 09 software.

Quantum Parameters	Neutral EDF	Protonated EDF
HOMO (eV)	-5.51846867	-5.913577965
LUMO (eV)	-0.15837025	-2.665899287
ΔE (eV)	5.36009842	3.247678678
Dipole Moment (μ)	6.3885	15.5051

The computational studies indicate towards the HOMO values that shows the electron donating tendency to the molecules ready to accept with vacant and low energy orbital. Meanwhile, the LUMO values indicate the inclination to accept electrons being the lower unoccupied orbitals [54]. The reactivity of the EDF molecules towards the steel surface is represented by the energy gap ΔE that serves to be an

important parameter. The computational calculations also confirm the relocation of electrons from the EDF molecules to the aluminium surface leading to the bond formation that inhibits corrosion [55].

4. CONCLUSIONS

- Expired drug Formoterol can be used as potential corrosion inhibitor for mild steel in 1 M H_2SO_4 solution.
- The weight loss tests showed that the corrosion rate declines in presence of EDF while the inhibition efficiency rises.
- The impedance studies revealed that the charge transfer resistance increases in presence of EDF.
- Polarization studies pointed that the anodic and cathodic shifts are mixed type in nature, so the EDF could be categorized in mixed class inhibitor.
- Contact angle showed the hydrophobic nature of the steel in presence of EDF. SEM showed the smooth mild steel surface with less roughness in presence of EDF.

ACKNOWLEDGMENT
We thank National Nature Science Foundation of China (51762042), Shaanxi Province Science and Technology Resources Open Sharing Platform Project (2019PT-18), Science and Technology Program of Shaanxi Province (2018GY-086, 2016GY-245，2017GY-131, and 2017JM2039),
Shaanxi Key Laboratory Project (19JS07), Technology Program of Yulin (2016CXY-03), and Transverse Research Projects of Yulin (2018HX08) for financial support.

References

1. M. Finšgar and J. Jackson, *Corros. Sci*., 86 (2014) 17.
2. R. Wang and S. Luo, *Corros. Sci*., 68 (2013) 119.
3. M. A. Bedair, M. M. B. El-Sabbah, A. S. Fouda and M. Elaryian, *Corros. Sci*., 128 (2017) 45.
4. K.C. Emregul and A. Abbas Aksut, *Corros. Sci.,* 42 (2008) 2051.
5. M.M. Solomon, S.A. Umoren, I.I. Udosoro and A.P. Udoh, *Corros. Sci*., 52 (2010) 1317.
6. L. Zhou, Y. L. Lv, Y. X. Hu, J. H. Zhao, X. Xia and X. Li, *J. Mol. Liq*., 249 (2018) 179.
7. A. A. Olajire, *J. Mol. Liq*., 248 (2017) 775.
8. Ambrish Singh, K. R. Ansari, M. A. Quraishi, Hassane Lgaz and Yuanhua Lin, *J. Alloys Comp*., 762 (2018) 347.
9. A. Singh, I. Ahamad and M. A. Quraishi, *Arab. J. Chem.*, 9 (2016) S1584.
10. A. Yousefi, S. Javadian, N. Dalir, J. Kakemam and J. Akbari, *RSC Adv*., 5 (2015) 11697.
11. Ambrish Singh, Yuanhua Lin, K. R. Ansari, M. A. Quraishi, Eno. E. Ebenso, Songsong Chen and Wanying Liu, *Appl. Surf. Sci*., 359 (2015) 331.
12. Ambrish Singh, Yuanhua Lin, M A Quraishi, Lukman Olasunkanmi, Omolola Fayemi, Sasikumar Yesudass, Ram Baskar, Indra Bahadur, Ime Obot, Abolanle Adekunle, Mwadham Kabanda and Eno Ebenso, *Molecules*, 20 (2015) 15122.
13. A. A. Khadom, A. N. Abd and N. A. Ahmed, *South African J. Chem. Eng*., 25 (2018) 13.
14. E. B. Ituen, O. Akaranta and S. A. Umoren, *J. Mol. Liq*., 246 (2017) 112.
15. M. M. Askari, S. G. Aliofkhazraei and A. Hajizadeh, *J. Nat. Gas Sci. Eng*., 58 (2018) 92.
16. A. Singh, Y. Lin, W. Liu, D. Kuanhai, J. Pan, B. Huang,C. Ren and D. Zeng, *J. Tai. Inst. Chem. E.*,

45 (2014) 1918.
17. Aijuan Zhao, H. Sun, L. Chen, Y. Huang, X. Lu, B. Mu, H. Gao, S.Wang and A. Singh., *Int. J. Electrochem. Sci*., 14 (2019) 6814.
18. Ambrish Singh, Y. Lin, W. Liu, S. Yu, J. Pan, C. Ren and D. Kuanhai, *J. Ind. Eng. Chem.*, 20 (2014) 4276.
19. D.D. Macdonald, S. Real and M. Urquidi-Macdonald, *J. Electrochem. Soc.,* 135 (1988) 2397.
20. D. Chu and R.F. Savinel, *Electrochim. Acta*, 36 (1991) 1631.
21. A.M. Abdel-Gaber, E. Khamis, H. Abo-ElDahab and Sh. Adeel, *Mater. Chem. Phys.*, 109 (2008) 297.
22. S.S. Zhang and T. R. Jow, *J. Power Sources*, 109 (2002) 458.
23. A.A. El Hosary, R.M. Saleh and A.M. Shams El Din, *Corros. Sci.*, 12 (1972) 897.
24. M.A. Quraishi, A. Singh, V.K. Singh, D.K. Yadav and A.K. Singh, *Mater. Chem. Phys*., 122 (2010) 114-122.
25. A. Singh, I. Ahamad, V.K. Singh and M.A. Quraishi, *J. Sol. State Electrochem*., 15 (2011) 1087.
26. G. Gunasekaran and L.R. Chauhan, *Electrochim. Acta*, 49 (2004) 4387.
27. Ambrish Singh, K.R. Ansari, Jiyaul Haque, Parul Dohare, Hassane Lgaz, Rachid Salghi and M.A. Quraishi, *J. Taiwan Inst. Chem. E*., 82 (2018) 233.
28. A.Y. El-Etre, M. Abdallah and Z.E. El-Tantawy, *Corros. Sci.*, 47 (2005) 385.
29. A. Singh, Y. Lin, I. B. Obot, E. E. Ebenso, K. R. Ansari and M. A. Quraishi, *Appl. Surf. Sci*., 356 (2015) 341.
30. E.E. Oguzie, *Corros. Sci*., 49 (2007) 1527.
31. Wang Xiaohong, Peng Zhengwei, and Ma Lai, *Int. J. Electrochem. Sci*., 12 (2017) 11006.
32. Xiqing Zhao, J. Xiong, S. Zhu, X. Zhao and A. Singh, *Int. J. Electrochem. Sci*., 14 (2019) 563.
33. I. B. Obot, Abdelkader Meroufel, Ikenna B. Onyeachu, Abdulrahmane Alenazi and Ahmad A. Sorour, *J. Mol. Liq*., (2019) 111760 https://doi.org/10.1016/j.molliq.2019.111760.
34. Z. Tao, S. Zhang, W. Li, and B. Hou, *Ind. Eng. Chem. Res*., 50 (2011) 6082.
35. E.S. Ferreira, C. Giacomelli, F.C. Giacomelli, and A. Spinelli, *Mater. Chem. Phys*., 83 (2004) 129.
36. A. Singh, K.R. Ansari, A. Kumar, W. Liu, C. Songsong and Y. Lin, *J. Alloys Comp*.,712 (2017)121.
37. D.D. Macdonald, *Electrochim. Acta*, 35 (1990) 1509.
38. K.-K. Lee and K.-B. Kim, *Corros. Sci*., 43 (2001) 561.
39. A. Singh, Y. Lin, E. E. Ebenso, W. Liu, J. Pan and B. Huang, *J. Ind. Eng. Chem*., 24 (2015) 219.
40. E. Khamis, *Corrosion*, 46 (1990) 476.
41. Ambrish Singh, V. K. Singh and M. A. Quraishi, *Arabian J. Sci. Eng*., 38 (2013) 85.
42. Vandana Saraswat and M. Yadav, *J. Mol. Liq*., (2019) 111883 https://doi.org/10.1016/j.molliq.2019.111883.
43. A. Singh, N. Soni, Y. Deyuan and A. Kumar, *Res. Phys*., 13 (2019) 102116.
44. X. Xu, A. Singh, Z. Sun, K. R. Ansari and Y. Lin, *R. Soc. Open Sci*., 4 (2017) 170933.
45. P. Singh, A. Singh and M.A. Quraishi, *J. Taiwan Inst. Chem. Eng*., 60 (2016) 588.
46. Y. Lin, A. Singh, E. E. Ebenso, Y. Wu, C. Zhu and H. Zhu, *J. Taiwan Inst. Chem. Eng*., 46 (2015) 214.
47. Ambrish Singh, K. R. Ansari, Dheeraj Singh Chauhan, M. A. Quraishi, H. Lgaz and Ill-Min Chung, *J. Col. Interf. Sci*., 560 (2020) 225.
48. A. Singh, Y. Lin, I. B. Obot and E. E. Ebenso, *J. Mol. Liq*., 219 (2016) 865.
49. K.R. Ansari, Dheeraj Singh Chauhan, M.A. Quraishi, Mohammad A.J. Mazumder and Ambrish Singh, *Int. J. Bio. Macromol*., 144 (2019) 305.
50. P. E. Alvarez, M. V. Fiori-Bimbi, A. Neske, S. A. Brandán and C. A. Gervasi, *J. Indus. Eng. Chem.*, 58 (2018) 92.
51. H. Feng, A. Singh, Y. Wu and Y. Lin, *New. J. Chem*., 42 (2018) 11404.
52. N. Li, S. Tang, Y. Rao, J. Qi, Q. Zhang and D. Yuan. *Electrochim. Acta*, 298 (2019) 59.

53. X. Wang, Z. Peng and S. Zhong, *Int. J. Electrochem. Sci*., 13 (2018) 8970.
54. Yang Yaocheng, Yin Caihong, Ambrish Singh and Yuanhua Lin, *New J. Chem*., 43 (2019) 16058.
55. A. Singh, K. R. Ansari, M. A. Quraishi, Savas Kaya and Priyabrata Banerjee, *New J. Chem*., 43 (2019) 6303.